

Low radiative efficiency accretion in the nuclei of elliptical galaxies

T.Di Matteo¹*, E.Quataert¹, S.W.Allen², R.Narayan¹ and A.C.Fabian²

1. Harvard-Smithsonian Center for Astrophysics, 60 Garden Street, Cambridge MA 02138

2. Institute of Astronomy, Madingley Road, Cambridge CB3 OHA

June 22, 2021

ABSTRACT

The discovery of hard, power-law X-ray emission (Paper I) from a sample of six nearby elliptical galaxies, including the dominant galaxies of the Virgo, Fornax and Centaurus clusters (M87, NGC 1399 and NGC 4696, respectively), and NGC 4472, 4636 and 4649 in the Virgo cluster, has important implications for the study of quiescent supermassive black holes. We describe how the broad band spectral energy distributions of these galaxies, which accrete from their hot gaseous halos at rates comparable to their Bondi rates, can be explained by low-radiative efficiency accretion flows in which a significant fraction of the mass, angular momentum and energy is removed from the flows by winds. The observed suppression of the synchrotron component in the radio band (excluding the case of M87) and the systematically hard X-ray spectra, which are interpreted as thermal bremsstrahlung emission, support the conjecture that significant mass outflow is a natural consequence of systems accreting at low-radiative efficiencies. We briefly discuss an alternative model for the observed X-ray emission, namely that it is due to nonthermal synchrotron-self Compton processes in the accretion flow, or wind. This appears to require implausibly weak magnetic fields. Emission from a collimated jet viewed off axis should be distinguishable from the bremsstrahlung model by variability and thermal line emission studies. We argue that the difference in radiative efficiency between the nuclei of spiral and elliptical galaxies arises from the different manner in which interstellar gas is fed into the nuclei. In ellipticals, matter fed from the hot (slowly cooling) ISM is likely to be highly magnetized and with low specific angular momentum, both of which favor low-radiative efficiency accretion solutions and possibly the formation of the observed jets.

Key words: galaxies: individual: M87 – NGC 1399 – NGC 4696 – NGC 4649 – NGC 4472 – NGC 4636, galaxies: active, accretion, accretion flows clusters: general – cooling flows – intergalactic medium – X-rays: galaxies

1 INTRODUCTION

The discovery of hard, power-law, X-ray emission associated with supermassive black holes in the nuclei of six nearby elliptical galaxies (Allen, Di Matteo & Fabian 1999; hereafter Paper I) has brought into sharper focus the issue of quiescent accretion and the potential ubiquity of low-level nuclear activity in early-type galaxies.

The nuclei of elliptical galaxies provide excellent environments for studying the physics of low-luminosity accretion. There is strong evidence, from high-resolution optical spectroscopy and photometry, that black holes with masses of 10^8 – 10^{10} M_\odot reside at the centers of bulge dominated

galaxies, with the black hole mass being roughly proportional to the mass of the stellar component (e.g. Kormendy & Richstone 1995, Magorrian *et al.* 1998; van der Marel 1998; Ho 1998).

X-ray studies of elliptical galaxies also show that they possess extensive hot gaseous halos that fill their gravitational potentials. Given the very large inferred black hole masses, this gas must inevitably be accreting at a rate which can be estimated from Bondi's (1952) spherical accretion theory (but, see Gruzinov 1999). Such accretion should, however, give rise to far more nuclear activity (e.g. quasar-like luminosities) than is observed if the radiative efficiency were as high as 10 per cent (e.g. Fabian & Canizares 1988), as is generally postulated in standard accretion theory.

Accretion with such high radiative efficiency need not necessarily occur in nearby ellipticals, however. The scheme

* Chandra Fellow

2 Low radiative efficiency accretion in the nuclei of elliptical galaxies

proposed by Rees *et al.* (1982; see also Begelman 1986; Fabian and Rees 1995) and successfully applied to a number of giant ellipticals in the Virgo cluster (M87: Reynolds *et al.* 1996; NGC 4649: Di Matteo & Fabian 1997a; Mahadevan 1997; Di Matteo *et al.* 1999, hereafter DM99) suggests that the final stages of accretion in elliptical galaxies may occur via an advection-dominated accretion flow (ADAF; Narayan & Yi 1995b; Abramowicz *et al.* 1995; for recent review see Narayan, Mahadevan & Quataert 1998). For such an accretion mode, the quiescence of the elliptical galaxy nuclei is not surprising; when the accretion rate is low, the radiative efficiency of the accreting (low density) material will also be low. Other factors may also contribute to the low luminosities observed. As discussed theoretically by Blandford & Begelman (1999; see also Narayan & Yi 1994; 1995a) and given observational credence by DM99, winds/outflows may transport energy, angular momentum and mass out of the hot, radiatively inefficient accretion flows, resulting in only a small fraction of the material supplied at large radii actually accreting onto the central black hole.

In fact, the central aim of this paper is to argue that the new X-ray (Paper I; and radio) constraints on nearby ellipticals provide strong support that a different accretion mode operates in these systems (as discussed also in Fabian & Rees 1995); this work also emphasizes the importance of mass loss in sub-Eddington, radiatively inefficient, accretion flows.

We present detailed models for the broad-band emission spectra of the same sample of six giant ellipticals studied in Paper I: M87 (also known as NGC 4486, the central galaxy of the Virgo Cluster), three other giant ellipticals in the Virgo Cluster (NGC 4649, NGC 4472 and NGC 4636; previously studied at high radio and sub-millimeter frequencies by DM99) and the central galaxies of the Fornax and Centaurus clusters (NGC 1399 and 4696, respectively). Hard power-law X-ray emission was recently discovered in all of these galaxies (Paper I). Most of the sources also show a noticeable lack of high frequency radio emission (DM99). Together with the absence of strong optical/UV flux (the “big blue bump”), or corresponding infrared (IR) flux (Paper I) this identifies these objects as a new class of accreting sources.

In Section 2, we will argue for low-radiative efficiency in the target sources by calculating the Bondi accretion rates and associated luminosities and showing that these latter values are much *greater* than those observed. We indicate also how radio and X-ray observations are crucial for constraining the properties of low radiative efficiency accretion. In §3 and §4 we summarize the data and the model calculations with particular emphasis on the effects of outflows on such models. Section 5 explicitly compares model predictions to the data and §6 provides some discussion of the implications for our models within the context of elliptical nuclei. Other possible contributions to the emission are briefly discussed in §7 and a prediction of the expected variability timescales is given in §8. We conclude and discuss our understanding of accretion from the hot ISM in elliptical nuclei in §9.

2 CLUES FOR UNDERSTANDING LOW RADIATIVE EFFICIENCY FLOWS

2.1 Black hole masses and accretion rates

The objects we consider are excellent examples of quiescent black holes. The radio galaxy M87 (NGC 4486), which lies at the center of the Virgo Cluster, has long been known to host a (low-luminosity) active nucleus, which powers both a relativistic jet and giant radio lobes. Both M87 and NGC 1399, the dominant galaxy of the Fornax Cluster, possess central, supermassive black holes with masses exceeding $10^9 M_\odot$ (Ford *et al.* 1994, Harms *et al.* 1994, Macchetto *et al.* 1997, Magorrian *et al.* 1998; see Table 1). Although no direct mass measurement for the central black hole in NGC 4696 has been made, this is the most luminous galaxy in our sample and is therefore likely to have the largest black hole. Both NGC 1399 and NGC 4696 also exhibit FR-I type radio activity.

The central cluster galaxies exist in highly gas-rich environments (*i.e.* in cooling flows at the centers of their host clusters; the integrated mass deposition rates from the cooling flows in and around M87 and NGC 4696 are $\sim 40 - 50 M_\odot \text{ yr}^{-1}$ (Allen *et al.* in preparation)). Although the other three Virgo ellipticals included in our sample (NGC 4649, NGC 4472 and NGC 4636) do not exist in such extreme environments, they also have measured black hole masses (Magorrian *et al.* 1998; also summarized in Table 1) and possess hot, rich, (also slowly cooling) X-ray emitting interstellar media (ISM) to feed the accretion flow.

Hot gas in the cooling flow or the potential well of the galaxy may be able to smoothly evolve into a hot, radiatively inefficient, accretion flow after it passes through the “Bondi accretion radius,” defined to be the point where the gravitational potential of the central black hole begins to dominate the dynamics of the hot gas; the accretion radius is given by $R_A \approx (c/c_s)^2 R_S$, where c is the speed of light, $c_s \sim 10^4 T^{1/2} \text{ cm s}^{-1}$ the sound speed (and T the gas temperature) and $R_S = 2GM/c^2$ the Schwarzschild radius of the black hole. As long as the cooling time for the gas is longer than the free fall time (*i.e.* the ISM density is low enough), the gas is able to stay hot as it passes through $\sim R_A$ and the accretion rate onto the black hole can be roughly calculated using Bondi’s (1952) formula, which requires an estimate of the density and temperature of the gas near $\sim R_A$.

We have carried out a deprojection analysis of *ROSAT* High Resolution Imager (HRI) observations for our sample of galaxies, with the primary aim of measuring the central X-ray emitting gas densities in these systems. The results (quoted at a fixed radius of 1 kpc) are summarized in Table 1. The inferred gas densities are relatively insensitive to assumptions about the underlying gravitational potential in the galaxies and host clusters and are typically characterized by an $R^{-\zeta}$ profile, where ζ is measured to be ~ 1 (Table 1). The measured densities for the central cluster galaxies are, as expected, slightly higher than for the Virgo ellipticals (see also Fig. 3, Paper I).

In order to estimate the accretion rates, we extrapolate the observed density profiles from 1 kpc to $\approx R_A$ using the power-law models listed in Table 1. For the systems of interest,

Table 1. Black hole masses (Magorrian et al. 1998), ISM densities, Bondi rates and radiative efficiencies

Object	Black Hole ($10^9 M_\odot$)	n_e (ISM) (cm^{-3}) at 1 kpc	ζ	\dot{M}_{Bondi} $M_\odot \text{ yr}^{-1}$	$L_{\text{Bondi}}/L_{\text{Obs}}$
M87	3.0	0.24	1.02	1.5	10^{-5}
NGC 1399	5.2	0.16	1.37	3	2×10^{-6}
NGC 4696	-	0.40	0.93	-	$\sim 10^{-5}$
NGC 4649	3.9	0.12	1.17	1.4	3×10^{-5}
NGC 4472	2.6	0.10	1.27	0.7	10^{-5}
NGC 4636	0.22	0.08	1.34	0.3	3×10^{-4}

$$R_A \sim 0.1 \left(\frac{M}{10^9 M_\odot} \right) \left(\frac{c_s}{300 \text{ km s}^{-1}} \right)^{-2} \text{ kpc.} \quad (1)$$

Thus, *ROSAT* observations at ≈ 1 kpc probe the gas structure reasonably close to R_A .

If the influence of the point mass becomes significant at a temperature T (where the ISM density $\rho_A = \rho(1 \text{ kpc})[1 \text{ kpc}/R_A]^\zeta$), the accretion rate is roughly given by

$$\dot{M} = 4\pi R_A^2 \rho_A c_s (R_A) \quad (2)$$

For M87 this implies an accretion rate

$$\begin{aligned} \dot{M} \sim & 10^{26} [1 \text{ kpc}]^\zeta c^{4-2\zeta} \left[\frac{n_e(1 \text{ kpc})}{0.24} \right] \\ & \left[\frac{c_s}{3.4 \times 10^7} \right]^{2\zeta-3} \left[\frac{R_S}{8.9 \times 10^{14}} \right]^{2-\zeta} \text{ g s}^{-1} \\ & \sim 1 M_\odot \text{ yr}^{-1}. \end{aligned} \quad (3)$$

The temperature of the interstellar medium, T , is assumed to be that determined from the ASCA analysis of the soft X-ray emission (Table 3, Paper I) for the Virgo ellipticals.[†] The ASCA spectra for the central cluster galaxies include a significant amount of emission from the extended cluster gas; the measured temperatures are therefore more likely to reflect the virial temperatures of the host clusters. Previous studies of M87 (e.g. Stewart et al. 1984), however, have shown that most of the gravitating mass in the central regions is associated with the galaxy itself rather than the Virgo cluster as a whole. For this reason, we assume a temperature $kT \sim 1 \text{ keV}$ for the central cluster galaxies (and for the deprojection analysis of the X-ray data in the innermost regions). This should better approximate the virial temperature of the galaxy potential in the inner regions (T should scale approximately with the square of the stellar velocity dispersion; the optical velocity dispersions for M87 and NGC 1399 are similar to those of NGC 4472 and NGC 4649 - Van der Marel 1991 - which have $kT \sim 1 \text{ keV}$; Paper I). The inferred Bondi accretion rates for NGC 4696 and NGC 1399 are of the same magnitude ($\sim 1 M_\odot \text{ yr}^{-1}$) as for M87, with slightly lower values for the Virgo ellipticals. Note that the gas densities at R_A , and the corresponding accretion rates, suggest that the systems are accreting at close to their upper limits. If we balance the cooling time (assuming a power

law approximation for the cooling rate; e.g. McKee & Cowie 1977) of the hot gas at $R \gtrsim R_A$ with the local free-fall time, then, from the Bondi theory, the maximum accretion rate is $\dot{M} \lesssim 3M_9 T_7^{1.6} M_\odot \text{ yr}^{-1}$, which is consistent with the assumption that gas will stay hot at $R \lesssim R_A$ and given our estimated accretion rates.

For the black hole masses determined for these galaxies (Table 1; Magorrian et al. 1998) accretion at the Bondi rate with a radiative efficiency of $\eta = 0.1$ (as assumed for standard accretion) would yield a luminosity ($\equiv L_{\text{Bondi}}$) exceeding $10^{46} \text{ erg s}^{-1}$ for central cluster galaxies (see Table 1). Observationally, the nuclei of these giant ellipticals are 4-6 orders of magnitude less active (see ratios of $L_{\text{Bondi}}/L_{\text{Obs}}$ in Table 1 and figures in Section 5). The observed luminosities of their cores do not exceed $10^{42} \text{ erg s}^{-1}$ for centre cluster galaxies and a few 10^{40} for the Virgo ellipticals (see also DM99 and the IR limits from Paper I). This provides strong observational evidence for low radiative efficiency accretion.

2.2 The spectrum of the accretion flow: testing the physics of low radiative efficiency accretion

In a low efficiency accretion flow around a supermassive black hole, the majority of the observable emission is in the radio and X-ray bands. In the radio band the emission results from cyclo-synchrotron emission due to the near equipartition magnetic field in the inner parts of the accretion flow. The X-ray emission is due either to bremsstrahlung or inverse Compton scattering. The cleanest test for probing the structure of low radiative efficiency accretion flows (i.e., ADAFs) is to examine the correlation between the radio and X-ray emission.

The self-absorbed synchrotron spectrum in an ADAF slowly rises with frequency in the radio band, up to some critical turnover frequency, typically in high radio to sub-mm frequencies, above which the emission should drop off quickly. The peak emission always arises from close to the black hole and reflects the properties of the accreting gas within a few Schwarzschild radii. Its Comptonization, which can dominate the X-ray emission, is also produced in the very inner regions of the flow. Bremsstrahlung emission, on the other hand, is typically produced at all radii in the flow.

The spectrum of a low efficiency accretion flow with a strong wind can be characterized by a variable accretion rate such that $\dot{M} \propto r^p$ where $p \sim 1$ (i.e. a large fraction of the mass supplied is carried away by the wind at large

[†] The temperature profile in the inner regions is the major uncertainty and may differ significantly due to local cooling or heating processes.

4 Low radiative efficiency accretion in the nuclei of elliptical galaxies

distances and only a small fraction is accreted). This implies a strong suppression of the synchrotron and Comptonized emission. However, relatively strong X-ray emission via bremsstrahlung can still occur (e.g. DM99; Quataert & Narayan 1999, hereafter QN99).

Assuming that the wind is spectrally unimportant (i.e. non-radiating) the importance of mass loss can be readily assessed by analyzing the correlation between the radio and X-ray emission in elliptical galaxies. If no wind is present and the accretion rate is of order the Bondi rate, the spectra should exhibit prominent synchrotron emission in the radio band and be dominated by Comptonization of this component in the X-ray band. Such systems would have relatively soft X-ray spectra. If, on the other hand, a significant outflow is present, the X-ray luminosity should dominate the radio luminosity and the X-ray spectrum should be very hard, as expected from bremsstrahlung emission.

Previous work has emphasized the power of radio and sub-mm observations of nearby ellipticals to test ADAF models. Such observations allow both the synchrotron flux and the position of the peak to be measured (DM99). In such work it was found that the predicted radio emission, based on the ADAF model (for magnetic fields in equipartition with thermal pressure and accretion at the Bondi rate), exceeds the measured fluxes by 2-3 orders of magnitude. Models with strong mass loss (winds), which can easily accommodate the observed suppression of the synchrotron emission, still predict a significant X-ray flux due to bremsstrahlung emission from the outer regions of the flows (if the accretion rates in these systems are similar to the Bondi value). The lack of any previous detection of nuclear X-ray emission (DM99), however, left open the possibility that the accretion rates in these systems were simply much lower than the Bondi value.

The discovery of hard power-law X-ray emission (Paper I) in the Virgo ellipticals studied by DM99 at the level of $10^{40} \text{ erg s}^{-1}$, and in three more central cluster galaxies with luminosities of up to $10^{42} \text{ erg s}^{-1}$, provides us with strong motivation to further consider low-radiative efficiency accretion models and in particular the evidence for mass outflow (note that throughout this paper we assume that the majority of the observed X-ray emission is from accretion onto the central supermassive black holes in these objects; see Section 4 of Paper I for the justification of this interpretation).

3 THE SPECTRUM OF THE CORE EMISSION

In order to examine the nature of accretion in the present sample of elliptical galaxies, we have compiled the best observational limits on the broad band spectra of their core emission. Our aim is to obtain good observational limits on the core flux over a wide range of frequencies rather than to compile a comprehensive list of all previous observations. Some contribution from the jets (particularly for the central cluster galaxies) and from the underlying galaxy are unavoidable; in some sense, then, the derived spectra should be considered as upper limits to the emission from the accretion flow.

The most up to date spectral energy distributions (SEDs) for the three Virgo elliptical galaxies (NGC 4649, NGC 4636 and NGC 4472) were compiled by DM99 (e.g. see

Tables 4,5 and 6 in DM99). These include stringent limits obtained at high radio and sub-millimeter frequencies with the Very Large Array (VLA) and SCUBA, respectively. The X-ray observations were upper limits obtained from ROSAT HRI. Here they are replaced with the ASCA detected hard power-law X-ray emission described in Paper I (the spectral slopes and luminosities in the 1-10 keV band are listed in Table 4 of that paper).

The spectral energy distribution for M87 (NGC4486) was previously compiled by Reynolds et al. (1996). Again, the X-ray observations have been updated to include the new ASCA (1-10 keV) data (Paper I, Table 4). We summarize the SEDs for NGC 1399 and NGC 4696 in Tables 2 and 3 respectively. The data for NGC 1399 also include new high radio frequency VLA data (consistent with a significant suppression of the high energy emission with respect to the standard ADAF model; Di Matteo, Carilli & Fabian in preparation). NGC 4696, the most luminous center cluster galaxy, is not as well constrained in the radio band and lacks a black hole mass measurement. According to the relationship $M_{bh} \propto M_{bulge}$ (e.g., Kormendy & Richstone 1995; Magorrian et al 1998; Ho 1998), however, it is expected to possess the the most massive black hole in our sample. Indeed, ASCA observations of NGC 4696 (Paper I) identify it as having the most luminous hard X-ray power-law emission.

3.1 Models

Accretion from the hot interstellar medium in elliptical galaxies (which should have relatively low angular momentum) may proceed directly into a hot, advection-dominated, regime.

When gas is supplied to a black hole at rates well below the Eddington rate it may not be able to radiate efficiently. In an advection dominated flow, which occurs at accretion rates $\dot{M} \lesssim \alpha^2 \dot{M}_{\text{Edd}}$, viscous stresses are assumed to dissipate most of the energy locally into the ions (a number of investigations have been carried out to study magnetic dissipation and particle heating in plasmas appropriate to ADAFs; e.g. Bisnovatyi-Kogan & Lovelace 1997; Quataert 1998; Gruzinov 1998; Blackman 1999; Quataert & Gruzinov 1999). A small fraction of the ion thermal energy is transferred to the electrons (which are responsible for the radiation) by Coulomb collisions, at a rate $\propto \dot{M}/\dot{M}_{\text{Edd}}\alpha^{-2}$. As a result of this poor thermal coupling (and the assumed ion heating), the radiative efficiency of the flow can be much less than the “canonical” disk value of $\sim 10\%$.

Narayan & Yi (1994,1995a) noted that ADAFs have the interesting property that the Bernoulli parameter, a measure of the sum of the kinetic energy, gravitational potential energy, and enthalpy, is positive over much of the flow; since, in the absence of viscosity, the Bernoulli parameter is conserved on streamlines, the gas can, in principle, escape to “infinity” with positive energy. Narayan & Yi speculated that this might make ADAFs a natural candidate for launching the outflows/jets seen to originate from a number of accretion systems. The positivity of the Bernoulli parameter, $Be > 0$ arises because viscous stresses transport energy and angular momentum from small radii to large radii in the flow (cf Narayan & Yi 1995 or Blandford & Begelman 1999). Consequently, the positivity of Be , and the result-

ing unboundedness of the “accreting” gas, is likely a generic feature of any hot, low radiative efficiency, accretion model.

Blandford & Begelman (1999) have recently suggested that mass loss via winds in ADAFs may be both dynamically crucial and quite substantial. They constructed self-similar ADAF solutions in which the mass accretion rate in the flow varies with radius R as $\dot{M} \propto R^p$ (see also simulations by Stone et al. in preparation). If the wind carries away roughly the specific angular momentum and energy appropriate to the radius from which it is launched, they show that the remaining (accreting) gas has a negative Bernoulli parameter only for large values of $p \sim 1$. Essentially, Blandford & Begelman suggest that $Be > 0$ is unstable. Matter will be lost to an outflow/wind in sufficient quantity to guarantee that the remaining matter is in fact bound, i.e., has $Be < 0$. In their view, then, outflows are inevitably driven by an accretion flow which cannot radiate. The outflow is necessary to guarantee that the accreting matter is bound to the central object. As we discuss in this paper, the radio observations of DM99 and the X-ray observations of Paper I provide support for this conjecture.

Numerical modeling techniques for ADAFs have advanced significantly during the last two years (see Narayan, Barret & McClintock 1997 and Esin McClintock & Narayan 1998). The calculations presented in this paper use such models and also include some modifications. One relevant difference here is the assumption that the mass inflow rate satisfies

$$\dot{M} = \dot{M}_{\text{out}} \left(\frac{R}{R_{\text{out}}} \right)^p \quad \text{for } R < R_{\text{out}}, \quad (4)$$

as in previous models by DM99 and QN99 ($\dot{M} = \dot{M}_{\text{out}}$ for $R > R_{\text{out}}$). The quantity \dot{M}_{out} is the accretion rate at the radius R_{out} where winds become important. Note that R_{out} need not be the same as R_A (the accretion radius), the radius at which the accretion flow starts.

The most relevant difference in the code is an improved calculation of the bremsstrahlung emissivity. Following previous work (Di Matteo & Fabian 1997; DM99) we now calculate the spectral emissivity using the expressions for the electron-electron bremsstrahlung and electron-ion bremsstrahlung computed by Stepney and Guilbert (1983). For the evaluation of the electron-ion bremsstrahlung (the dominant contribution), it is important to use the cross section in the Born approximation for a relativistic electron in a Coulomb field given by Gould (1980). For electron-electron bremsstrahlung process, the cross-section is much more complicated and we have used the numerically integrated expression given in Stepney and Guilbert (1983). The resulting emissivity includes both contributions.

For convenience and consistency with previous work we scale black hole masses in solar units, $M = m M_{\odot}$, and accretion rates in Eddington units, $\dot{M} = \dot{m} \dot{M}_{\text{Edd}}$ and $\dot{M}_{\text{Edd}} = L_{\text{edd}}/0.1c^2$. We rescale the radial co-ordinate in Schwarzschild units, $R = r R_s$.

The ADAF model is specified by four parameters: α , the viscosity parameter, β , the ratio of gas to magnetic pressure, γ , the adiabatic index of the fluid, which is assumed to be $5/3$, and δ , the fraction of the turbulent energy which heats the electrons. The thermodynamic state of the flow is described by the ion temperature $T_i \sim 10^{12} \beta r^{-1}$ K (which is to a very good approximation the virial temperature), the

electron temperature, T_e , and the magnetic pressure. The electron temperature profile is obtained by solving the full electron energy equation, including the electron entropy gradient (Nakamura et al. 1997; Esin et al. 1997; Narayan et al. 1998)

The microphysical parameters in ADAFs are quite uncertain; unless otherwise specified we take $\beta = 10$, $\alpha = 0.1$ (in accordance with the viscosity parameter scaling roughly as $\alpha \sim 1/\beta$, as expected if turbulent stresses arise solely from magnetic fields; Hawley, Gammie & Balbus 1996), and $\delta = 10^{-2} - 0.1$ (as we shall show later the observational constraints allow us to vary the fraction of electron heating with no significant modification to any of the conclusions). Excepting α (which is discussed in §7), the particular values assumed for these parameters are not important for any of our qualitative conclusions. Variations in the predicted spectrum due to changes in the microphysical parameters have been investigated by QN99.

The other model parameters are m , which is estimated from observations (apart from NGC 4696), p , r_{out} and \dot{m}_{out} . \dot{m}_{out} is adjusted to reproduce the X-ray data. The predicted spectrum depends primarily on the fraction of the incoming mass accreted onto the central object, so that p and r_{out} are somewhat degenerate. They can, however, be decoupled to some extent when one attempts to satisfy both the radio and X-ray constraints.

4 SPECTRA OF ADAFS WITH WINDS

ADAF models with a variable accretion rate have been investigated by DM99 in the context of elliptical galaxy nuclei and in greater detail and generality by QN99. Here we will briefly summarize how the different spectral features are affected by the presence of outflows. In the magnetized, optically thin plasma of an ADAF, with an electron temperature of $10^9 - 10^{10}$ K, the most important radiation processes are synchrotron emission, Compton scattering and bremsstrahlung emission.

We will use the self-similar approximation to indicate how the introduction of a radially varying \dot{m} (see Eqn. 1) changes the predicted spectrum. As mentioned earlier, in the thermal plasma of an ADAF, synchrotron emission rises steeply with increasing frequency. Under most circumstances the emission becomes self-absorbed and gives rise to a black-body spectrum below a critical frequency, ν_c . Above this frequency it decays exponentially as expected from a thermal plasma. The peak frequency scales as $\nu_c \propto BT_e^2 \propto m^{-1/2} \dot{m}^{1/2} T_e^2 r^{-5/4}$ and the luminosity (approximated by the Rayleigh-Jeans limit) varies as (Mahadevan 1997)

$$\nu_c L_{\nu c} \propto \nu_c^3 T_e m^2 r^2 \propto \beta^{-3/2} T_e^7 \dot{m}^{3/2}. \quad (5)$$

Note that emission observed at higher frequencies originates at smaller radii and that the total power is a very strong function of temperature.

For all other model parameters fixed, the predicted synchrotron emission decreases strongly with the introduction of a wind (i.e., with increasing p). There are two reasons for this. First, increasing p decreases the magnetic field strength near $r \sim 1$, where the high frequency synchrotron emission originates (this is because the density and the gas pressure

6 Low radiative efficiency accretion in the nuclei of elliptical galaxies

decrease as p increases). In addition, the electron temperature decreases as p increases. This is because adiabatic compression of the electrons is less efficient (when p is large, the density profile is flatter, and hence T_e is smaller). By equation (5), the synchrotron emission is particularly sensitive to the electron temperature. Therefore, the synchrotron emission falls very rapidly with increasing p .

The Compton power, i.e., the Compton scattering of soft synchrotron photons by the hot electrons in the accreting gas, decreases with increasing p even more strongly than the synchrotron does. The optical depth to electron scattering decreases with the introduction of a wind, as does the electron temperature. In other words, the Compton- y parameter $\sim 16(kT_e/m_e c^2)\tau$ is $\ll 1$ in ADAFs with outflows.

In contrast to the processes discussed above, bremsstrahlung emission arises from all radii in the flow. The emission at frequency ν is, however, dominated by the largest radius which satisfies $h\nu \sim kT(r)$. The large radii dominate because, so long as $h\nu \lesssim kT$, the bremsstrahlung luminosity from a spherical shell of radius r and thickness $dr \sim r$ is $\propto r^3 \rho^2 T^{-1/2} \propto r^{2p} T^{-1/2}$ which is an increasing function of r (even for $p = 0$). Note that the radial dependence of the emissivity depends on the density profile of the flow and therefore on the strength of the wind. This is seen explicitly in Figure 1 which shows the bremsstrahlung emissivity, ϵ_ν (ergs s^{-1} Hz $^{-1}$), as a function of r for 3 different X-ray energies (from top to bottom, 1, 10, & 100 keV). The solid lines show a no-wind ADAF model while the dotted lines show an ADAF model with $p = 0.5$ and $r_{\text{out}} = 10^3$ (this model is favored by the observations discussed in §5). Note that the soft X-ray emission is always dominated by radii $\sim 10^3 - 10^4 R_S$ since this is where $kT \sim$ a few keV. Even in the absence of a wind, the hard X-ray emission is dominated by radii $\gtrsim 100 R_S$ since $kT \gtrsim 100$ keV for $r \lesssim 10^2 - 10^3$. In the presence of a wind, radii $\lesssim r_{\text{out}}$ contribute negligible to the bremsstrahlung emission.

As pointed out by QN99 (and explicitly shown in Figure 1), bremsstrahlung emission at 1 – 10 keV is rather insensitive to the presence of a wind since it originates from the outer regions of the flow. X-ray observations in this band can therefore directly measure the density at the outer edge of the flow and provide a firm estimate of the rate at which matter is fed to the accretion flow (i.e. \dot{m}_{out}). At energies around 10 keV and above, the bremsstrahlung emission would decrease with increasing p if the outflow were to start at $r_{\text{out}} \sim 10^4$. The absence of a decrease in the thermal bremsstrahlung emission at and above 10 keV (cf §5) therefore implies either that there is no wind or that the outflow starts at radii $\ll 10^4$.

5 COMPARISON WITH THE DATA

Figure 2 shows the observational constraints on the spectra of the six giant elliptical galaxies together with our model predictions. A striking feature of the broad band spectral energy distributions is the “non-thermal” character of the emission. In particular, it is apparent that most of the luminosity is produced in the X-ray band (very hard energy spectral slopes are observed ranging from $\alpha_x \sim 0.4$ to -0.3), with roughly two orders of magnitude less luminosity coming out in the radio band. (The case of M87 is less drastic,

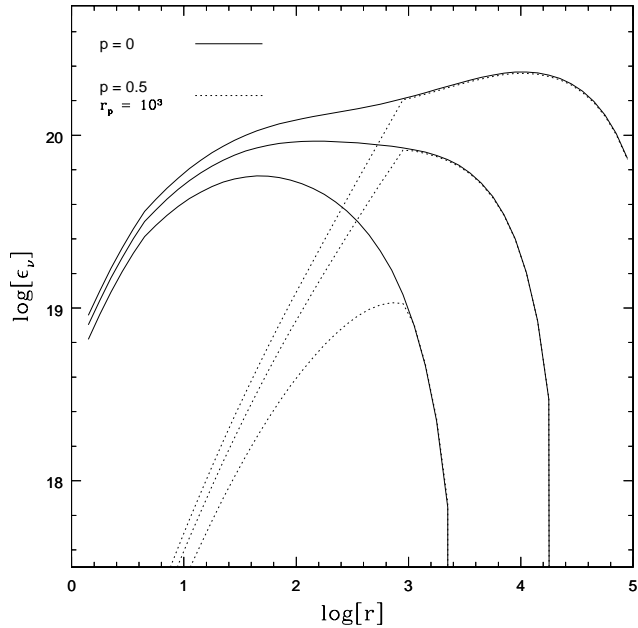


Figure 1. The bremsstrahlung emissivity, ϵ_ν (ergs s^{-1} Hz $^{-1}$), as a function of r for three different X-ray energies (from top to bottom, 1, 10, & 100 keV). The solid lines show the bremsstrahlung emission for a no-wind ADAF model while dotted ones show an ADAF model with a wind characterized by $p = 0.5$ and $r_{\text{out}} = 10^3$ (observationally favored parameters; see Section 5).

with the X-ray luminosity exceeding that in the radio band by less than a factor 10. The results for NGC 4696 are also more uncertain due to the lack of any high frequency radio data). The SEDs are very different from those of standard AGN, which are typically much flatter (in νL_ν) with big blue bumps in the optical/UV bands (generally interpreted as thermal emission from a standard thin disk) and X-ray emission with slopes of $\alpha_x \sim 0.8 - 1$.

In the following Sections, we present detailed models for each of the galaxies in our sample. The results shown in the figures, for various values of p , all have $\alpha = 0.1$, $\beta = 10$ and $\delta = 0.01$ (or 0.1). The value of \dot{m}_{out} is adjusted to fit the observed ASCA X-ray flux at 1 keV. These measurements are then compared to the predicted Bondi accretion rates to check for consistency. In all of the models p is required to be large enough to satisfy the stringent radio limits (for NGC 1399, NGC 4649, NGC 4472 and NGC 4636). We shall show that this also yields a bremsstrahlung dominated X-ray spectrum (as required independently by the ASCA data). We start by describing the spectral models for each object and then discuss the general picture which arises from the comparison with the data.

5.1 Central cluster galaxies

5.1.1 M87

Figure 2a shows the spectral models for M87 for different values of p and r_{out} . The high frequency radio data (unlike in most of the other galaxies) is completely consistent with a model with no wind, i.e. $p = 0$. In this case, however, the

X-ray emission is due to Comptonization of the synchrotron photons. The predicted slope is too soft to be consistent with the ASCA data (dashed line Fig. 2a). The accretion rate in this case is $\dot{m} = \dot{m}_{\text{out}} \sim 10^{-3}$. This model also predicts an optical flux (due to the first Compton bump) which exceeds the HST limit: a further increase in \dot{m} , which seems to be required by the X-ray data, would significantly violate this limit.

The dotted line shows a model for $r_{\text{out}} = 10^4$ and $p = 0.37$ (which has $\dot{m}_{\text{out}} = 0.025$). Although this model has the correct hard slope up to $\sim 5 - 7$ keV, the effects of a wind starting at $r = 10^4$ introduce a fairly strong suppression of the X-ray emission above ~ 5 keV (a spectral break in the bremsstrahlung emission as described in §4). The best fit model (solid line) shows the effects of reducing r_{out} to ~ 300 (with $p = 0.45$ and $\dot{m}_{\text{out}} = 0.015$). In fact, good agreement with the X-ray data is obtained for any $r_{\text{out}} \lesssim 1000$. The quoted values for r_{out} should only be considered accurate to order of magnitude, but values of $\sim 10^2 - 10^3$ are preferred for all systems we consider (see the comparison between the solid, dotted and dashed lines in Fig. 2a).

In the models with winds, the 100 GHz VLBI data might require an additional component; the synchrotron jet or the wind itself could be candidates; note also that increasing δ (with a relative increase in p so that the X-ray emission is still dominated by bremsstrahlung), *e.g.*, further electron heating in reconnection sites, would increase the electron temperature and therefore the synchrotron flux by a factor $\propto T_e^7$. This might produce the required radio flux as well (see also Fig. 2d for NGC4649).

5.1.2 NGC 1399

Fig. 2b shows three spectral models for NGC 1399. Both the high frequency VLA data and the ASCA spectral slope are inconsistent with the $p = 0$ model (dashed line). Also, the very hard X-ray slope is best accounted for by a model with larger p and smaller r_{out} so that no spectral break is introduced around $\sim 6 - 8$ keV (thinner solid line: $r_{\text{out}} = 10^4$, $p = 0.4$, $\dot{m}_{\text{out}} \sim 9 \times 10^{-3}$). A model which is consistent with both the suppression of synchrotron radiation in the radio and the hard slope in the X-ray band has $r_{\text{out}} = 300$, $p = 0.6$, and $\dot{m}_{\text{out}} \sim 5 \times 10^{-3}$ (thicker solid line in Fig. 2b).

5.1.3 NGC 4696

We do not have an estimate of the black hole mass in NGC 4696. Given that this is the most luminous and massive galaxy in the Centaurus cluster we will assume that its black hole mass is comparable to that of M87 or NGC 1399. In detail, we assume $m \sim 5 \times 10^9$ (which is roughly consistent with the radio data). No high frequency radio data are available for this object and the only important constraint is given by the ASCA observations. The relatively high flux and hard X-ray ray slope can be accounted for by models with $p \sim 0.6$ and $r_{\text{out}} \sim 300$ (thicker solid line Fig. 2c). This implies $\dot{m}_{\text{out}} \sim 0.03$. Models with no wind would again predict Compton dominated spectra with slopes too soft to explain the ASCA observations (dashed line, Fig. 2c).

5.2 Virgo ellipticals

5.2.1 NGC 4649

NGC 4649 has the best observational constraints of any object in the sample. The radio data for this object show a very point-like source, dominated by its core component at high radio frequencies. The VLA 22 to 43 GHz data points and the SCUBA sub-mm upper limit at (10^{11} Hz) also imply a very sharp spectral turnover in the radio spectrum which is hard to explain with any non-thermal particle distribution, but easily obtained from thermal synchrotron radiation (DM99). The flux in the radio-sub-mm band is orders of magnitude below that expected from models without winds, but is easily matched by models with winds (see Fig. 2d and 5 in DM99). The value of p required to account for the (lack of) radio emission (~ 0.4) would produce a significant spectral break in the high energy X-ray band due to the suppression of the higher temperature (inner radii) bremsstrahlung if $r_{\text{out}} \sim 10^4$. Better agreement with the data is again obtained by taking $r_{\text{out}} \sim 300$ and $p \sim 0.5$, which imply $\dot{m}_{\text{out}} \sim 2.7 \times 10^{-3}$ (thicker solid line, Fig. 2d). The dash-dotted line shows a models for $\delta = 0.1$. The increased electron heating in models with winds implies a slight increase in p in order to re-establish agreement with the radio constraints ($p = 0.8$; a slight decrease of r_{out} might also be necessary for the high energy X-ray data). Note that models with winds (as required by the observational constraints) can easily allow for different fractions of electron heating with no significant change to any of our conclusions (see QN99 for a general discussion of this point).

5.2.2 NGC 4472

Although the VLA and SCUBA sub-mm data do not imply a very sharp spectral turnover in this object, they require significant suppression of the emission from the inner regions of the flow, as expected in the presence of a strong wind. These limits, together with the ASCA X-ray flux and spectral index, also prefer models for which $r_{\text{out}} \sim 300$ and imply $p \sim 0.5$ and $\dot{m}_{\text{out}} \sim 5 \times 10^{-3}$ (see Fig. 2e).

5.2.3 NGC 4636

NGC 4636 is the only object in this sample with $m < 10^9$. The relatively small black hole mass, as estimated by Magorrian et al. (1998), and the relatively high accretion rates required to fit the ASCA X-ray flux measurement, shift the synchrotron peak to higher frequencies than those expected by the radio and sub-mm measurements (Fig. 2f dashed lines).[‡] In this case, the X-ray spectral slope and flux do not constrain r_{out} . Models with $r_{\text{out}} = 10^4$ ($p = 0.55$ and $\dot{m}_{\text{out}} = 0.03$) and $r_{\text{out}} = 300$ ($p = 0.9$ and $\dot{m}_{\text{out}} = 0.018$) provide satisfactory fits to the X-ray data.

Note that an increase in the black hole mass to $m \sim 10^9$ (similar to the other objects) would shift the synchrotron peak to lower frequencies and into good agreement with the

[‡] In DM99 the much lower accretion rate and differences in the electron temperature could accommodate the peak position as set by the data.

8 Low radiative efficiency accretion in the nuclei of elliptical galaxies

radio limits (solid lines in Fig. 2f). The very sharp spectral turnover implied by the VLA observations can otherwise only be explained by a very peculiar distribution of non-thermal particles with a very sharp cut off at relatively low gamma or by an additional thermal synchrotron component in the jet or wind.

We now turn to the general conclusions which can be drawn from our modeling of the six nearby elliptical galaxies and a brief discussion of the crucial properties of their environments and their influence on the accretion flows.

6 LOW RADIATIVE-EFFICIENCY ACCRETION AND COOLING FLOWS IN ELLIPTICALS

The broad band spectra of the six nearby elliptical galaxies are characterized by one or both of the following properties: a large X-ray to radio luminosity ratio (with indications of a sharp spectral cut-off in the radio) and a hard X-ray spectral index. These point to the importance of outflows in low luminosity systems. The strong synchrotron peak in the radio, expected to dominate the broad band emission, is strongly suppressed. The X-ray emission is typically extremely hard and is well explained by bremsstrahlung emission.[§] As discussed in Section 4, the introduction of a wind accounts for these characteristic spectral features. Note also that these conclusions are not dependent on the choice of the microphysical parameters (although high values α are required for consistency); in particular it is worth noting that significant electron heating ($\delta \gtrsim 0.1$) is perfectly viable.

The only object which does not show a spectral turnover at high radio frequencies and which therefore does not require a mechanism to suppress the radio emission is M87 (apart from NGC 4696, for which no data is available to constrain the high frequency emission). Recall that this is the only object in our sample with a one sided jet which is most probably relativistically beamed towards us (and, in particular, M87 is among the more active FR-I radio sources in central cluster galaxies). As shown by the radio map of Baath et al. (1992) the jet is resolved by high resolution VLBI 100 GHz observations together with the core. As we shall discuss later, contributions from such a jet might even be important for what we are labeling accretion flow emission. Nevertheless, models which do not include significant mass loss are unable to explain the hard X-ray spectral slope, which is easily accounted for by bremsstrahlung emission.

6.1 Outer Radii and Angular Momentum

The amount of mass loss required to satisfy the X-ray to radio flux ratio and/or the observed X-ray slope would give rise to a cut-off in the bremsstrahlung emission at energies

[§] The X-ray spectra of several of the sources are actually slightly harder than expected from thermal bremsstrahlung emission (i.e. in $\nu L_\nu \propto \nu$ for $kT_e < h\nu$). We expect that small amounts of intrinsic absorption are responsible, since the observed slopes are too hard to arise from any other likely process e.g. photon starved thermal Comptonization, or non-thermal Comptonization; see also the infra-red (IRAS) limits presented in Paper I.

$\lesssim 10$ keV (apparently inconsistent with the ASCA data) were the outflow to start at radii $r \gtrsim 10^4$. Better agreement with the X-ray observations is obtained for outflows starting inside the outer boundary of the flow at radii $\lesssim 10^3$.

This result may suggest that angular momentum does not dominate the flow close to the accretion radius, perhaps because angular momentum in the hot gas is transported outward in the halo by turbulence (Nulsen, Stewart & Fabian 1984) or because the hole is moving with respect to the gas. (In order that the gas shed at large radii may flow unimpeded to the centre of the galaxy, its angular momentum must be dissipated. A rotating, contracting flow - as a cooling flow in an elliptical galaxy - is very likely to become turbulent. Angular momentum must then be transported efficiently outside the medium and is likely to be taken up by some parts of the shed gas - as the gas flows in). The inflow across the accretion radius could then be roughly spherically symmetric with the specific angular momentum being a fraction, ξ , of the one required for a Keplerian orbit at $R \lesssim R_A$. In particular, in order for the angular momentum dominated flow to start at $r \sim r_{out} \sim \xi^2 r_A \sim 10^3$, ξ must be $\lesssim 0.03$ (radial accretion is precluded unless $\xi \leq 10^{-3}$). Further investigations both on the theoretical and observational side are necessary to more carefully assess the values of r_{out} and the above hypothesis.

We now briefly discuss how the gas densities (i.e the rates at which matter is fed at r_{out}) required to explain the observed X-ray fluxes compare to the expected Bondi rates.

6.2 Accretion Rates and magnetic fields in the central regions

The accretion rates for each model are obtained by normalizing the model to the measured X-ray fluxes. The results for all of the models shown in Fig. 2 are tabulated in Table 4. The accretion rates required to explain the X-ray fluxes are consistent with the Bondi values predicted in Section 1.1 from the deprojection analysis of the X-ray gas. The differences in accretion rates, for a given object and X-ray flux, with varying r_{out} and p are mostly from the slightly different electron temperature profiles in such models. We also note that the accretion rates implied by models with no wind would be smaller by roughly an order of magnitude. The X-ray flux in all such models is, however, due to inverse Compton scattering of the synchrotron photons. In no case can a Compton-dominated ADAF model give a satisfactory fit to the radio and X-ray observations.

The Bondi accretion rates previously estimated for M87 by Reynolds et al. (1996) and for the Virgo ellipticals by DM99 are typically a factor 5-8 lower than the ones presented in Section 1.1. The differences in the calculations arise from the fact that we now take into account that the X-ray gas density rises with decreasing radius as $n \propto r^{-1}$. Near the accretion radius it is typically larger by a factor of few than at ~ 1 kpc (used by the above authors). Although the spatial resolution of the ROSAT HRI does not allow us to directly probe the accretion radii in these objects (0.03–0.05 kpc) the observed density profiles are very well fitted by the power-law models (as detailed in Table 1) between radii of 7 – 10 kpc down to 0.2 – 0.5 kpc. The density estimates indicate that accretion rates of order $0.5 – 2 M_\odot \text{ yr}^{-1}$ are perfectly plausible in these systems.

Table 2. Summary of data for the core of NGC 1399.

Frequency ν (Hz)	νF_ν (10^{-15} erg s $^{-1}$ cm $^{-2}$)	reference	notes
2.3×10^9	0.35	Slee et al. (1994)	PTI
4.9×10^9	0.50	Sadler et al. (1989)	VLA
8.4×10^9	1.68	Slee et al. (1994)	PTI
8.4×10^9	1.81	Di Matteo et al. (1999)	VLA
2.2×10^{10}	5.60	Di Matteo et al. (1999)	VLA
4.3×10^{10}	7.10	Di Matteo et al. (1999)	VLA
2.4×10^{17}	98	Paper I	ASCA
2.4×10^{18}	1350	Paper I	ASCA

PTI: Parkes-Tidbinbilla interferometer

Table 3. Summary of data for the core of NGC 4696.

Frequency ν (Hz)	νF_ν (10^{-15} erg s $^{-1}$ cm $^{-2}$)	reference	notes
2.3×10^9	0.57	Slee et al. (1994)	PTI
4.9×10^9	2.70	Sadler et al. (1989)	VLA
8.4×10^9	1.17	Slee et al. (1994)	PTI
2.4×10^{17}	358	Paper I	ASCA
2.4×10^{18}	6221	Paper I	ASCA

PTI: Parkes-Tidbinbilla interferometer

Table 4. Model parameters for Fig. 2

Object	r_{out}	p	\dot{m}_{out}	Line type
M87	10^4	0	10^{-3}	dashed
	10^4	0.37	0.03	thin solid
	800	0.4	0.017	dotted
	300	0.45	0.015	thick solid
	100	0.5	0.013	dotted
	10^4	0	0.7×10^{-3}	dashed
NGC 1399	10^4	0.44	0.01	thin solid
	300	0.6	6.7×10^{-3}	thick solid
	10^4	0	1.4×10^{-3}	dashed
NGC 4696	10^4	0.4	0.05	thin solid
	300	0.62	0.03	thick solid
	10^4	0	4×10^{-4}	dashed
NGC 4649	10^4	0.38	4.4×10^{-3}	thin solid
	300	0.52	2×10^{-3}	thick solid
	100	$0.8(\delta = 0.1)$	$2.5 \times 10^{-3} (\delta = 0.1)$	dot-dashed
	10^4	0	5×10^{-4}	dashed
NGC 4472	10^4	0.37	8×10^{-3}	thin solid
	300	0.5	5×10^{-3}	thick solid
	10^4	0	$10^{-3} (4 \times 10^{-4})$	dashed
NGC 4636	10^4	0.55 (0.5)	$0.03 (6 \times 10^{-3})$	thin solid (short dashed)
	300	0.9 (0.62)	$0.018 (3 \times 10^{-3})$	thick solid (short dashed)

 Notes: The values of p and \dot{m}_{out} in brackets, for NGC 4636, refer to those obtained assuming $m \sim 10^9$, see also Fig 2f.

The gas densities at R_A , estimated in Section 2, and the corresponding accretion rates and best-fit model predictions indicate that the systems are accreting at close to their upper limits implied by cooling. The main uncertainty in the calculation of \dot{m} in these systems - given the measured black hole masses - are the estimates of the temperature of the cooling flows near the accretion radii. As discussed by Gruzinov (1999; and along the same lines by Ostriker et al. 1976) turbulent heat conduction may cause the flow to become hotter and hinder accretion (although heat conduction is likely to be suppressed in a magnetized cooling flows; see Chandran, Cowley & Sydora 1998). Alternatively, thermal instabilities may set up near the sonic point and remove lots of the gas - although a central point mass would eventually re-suppress the instability at small radii. These issues might be more easily addressed observationally in the near future with high spatial resolution X-ray observations made with the Chandra Observatory, which will determine the temperature profiles in elliptical galaxies on spatial scales approaching the accretion radius.

Given that the accretion rates in the ellipticals are similar to those in Seyfert galaxies and other active nuclei, it is puzzling why these objects should exhibit such different behavior. The different environments in the galaxies may play a major role (see Fabian & Rees 1995; Begelman 1986; Rees et al. 1982). When accretion proceeds from the (already hot) interstellar medium (with relatively low angular momentum) the resulting quasi-Bondi flow may go directly into a hot, radiatively inefficient solution. Such a solution might be preferentially obtained in elliptical galaxies because the magnetic field strengths can be typically much higher and close to equipartition values, even outside the accretion radius (when the material has participated in a cooling flow; Soker & Sarazin; 1990). An initially weak magnetic field can be dramatically increased by the radial inflow and shear in a cooling flow (or any spherical inflow; Shapiro 1973; Meszaros 1975) - the combination of transverse compression and radial compression can enhance the magnetic stresses proportionally to r^{-4} , whereas the gas pressure goes no more steeply than $r^{-5/2}$. The magnetic field is built up to equipartition values even before it reaches the accretion radius. If the material enters the accretion flow with close to equipartition magnetic fields, it might be more likely to accrete directly in a high- α flow (as α is expected to scale with β ; e.g. Hawley, Gammie & Balbus 1996). Higher viscosity (if $\alpha \gtrsim 0.1$ can be achieved) would then allow the systems to be radiatively inefficient. The presence of relatively large scale (mostly radial) magnetic fields might also be important as an agent for launching the wind itself. Finally, since at large distances from the disk the inertia of the gas can cause the magnetic field to become increasingly toroidal, the magnetic stresses could also be responsible for converting the centrifugal outflow into a more collimated jet structure (as observed in the different degrees of radio activity in most of the ellipticals).

7 ALTERNATIVES TO THE WIND MODEL

7.1 The Bremsstrahlung Interpretation

It is worth being slightly more explicit about precisely what is required to reconcile the basic ADAF model of Narayan &

Yi (1995b) with the radio (DM99a) and X-ray observations (Paper I) of nearby elliptical galaxies.

In particular, we have been arguing as if the bremsstrahlung interpretation of the observed hard X-rays fixes the accretion rate to be \sim the Bondi rate. This is not strictly correct; the bremsstrahlung luminosity depends only on the gas density and temperature, not on the accretion rate. What the X-ray observations fix, then, is $\rho(R_{\text{out}}) \propto \dot{M}(R_{\text{out}})/|v_r(R_{\text{out}})|$ where $v_r(R_{\text{out}})$ is the radial velocity of the gas near the outer radius of the accretion flow. The Bondi solution has $v_r \approx v_K$ while the ADAF solution has $v_r \approx \alpha v_K$, where v_K is the Keplerian or free fall velocity at R_A . Consequently, the X-ray observations fix $\dot{M}(R_{\text{out}})/\alpha$ (cf Narayan & Yi 1995b).

The radio observations, on the other hand, are sensitive to $\rho(R_{\text{in}})$ and $T_e(R_{\text{in}})$, the flow properties close to the black hole. Since $v_R \sim c$ near the black hole (gas flows through the horizon at the speed of light), the radio observations indeed fix $\dot{M}(R_{\text{in}})$ (given α, β, δ , etc. which fix T_e). In fact, they fix $\dot{M}(R_{\text{in}})$ to be $\ll \dot{M}_{\text{Bondi}}$.

In the previous subsection, we emphasized that the accretion rates necessary to explain the X-rays as bremsstrahlung are comparable to the Bondi value. This is, however, for $\alpha \approx 0.1$ (the value chosen here). If α were to be $\ll 1$, the accretion rates consistent with the X-ray observations would also be $\ll \dot{M}_{\text{Bondi}}$. Consistency with the observations would require $\alpha \sim 10^{-4} - 10^{-3}$. In light of recent work on MHD turbulence and angular momentum transport in accretion flows (Balbus & Hawley 1998; Hawley, Gammie, & Balbus 1996), we do not think that small α due to small viscosity is a viable possibility. A more interesting possibility is a suggestion due to Gruzinov (1999). He pointed out that if there is significant radial heat conduction in a Bondi-type flow, it can lead to a strong suppression in the radial velocity of the accreting material near R_A . Thus, even in the absence of viscosity (Gruzinov's model was non-ideal but inviscid), the radial velocity may be much smaller than the free fall value. His model could, on these grounds, account for the observations of nearby ellipticals as well as the wind model we have been emphasizing (without any outflow).

There is, however, one argument which we believe rules out Gruzinov's proposal as a complete explanation for the observations of DM99 and Paper 1. Namely, any model with $\alpha \ll 1$ which produces X-ray luminosities comparable to those observed will have a cooling time much shorter than the inflow time of the gas and will therefore cool catastrophically to a thin disk. More concretely, only for $\dot{m}(R_{\text{out}}) \lesssim \alpha^2$ can cooling be neglected in the dynamics of the flow (as is done in the ADAF and Bondi solutions). The bremsstrahlung interpretation of the X-rays from nearby ellipticals fixes $\dot{m}(R_{\text{out}})/\alpha$ to be ~ 0.1 (cf Table 4 and recall that those models took $\alpha = 0.1$). Consequently, only models with $\alpha \gtrsim 0.1$ are consistent hot accretion flow models for the systems at hand. This rules out any solution, including Gruzinov's, which appeals to a low radial velocity near R_A . If indeed heat conduction (or other mechanisms) reduces $\dot{M}(R_{\text{out}}) \ll \dot{M}_{\text{Bondi}}$ (but α is still ~ 0.1) the observed X-ray flux (and the radio one, if the decrease is very severe) must be produced by processes other than bremsstrahlung.

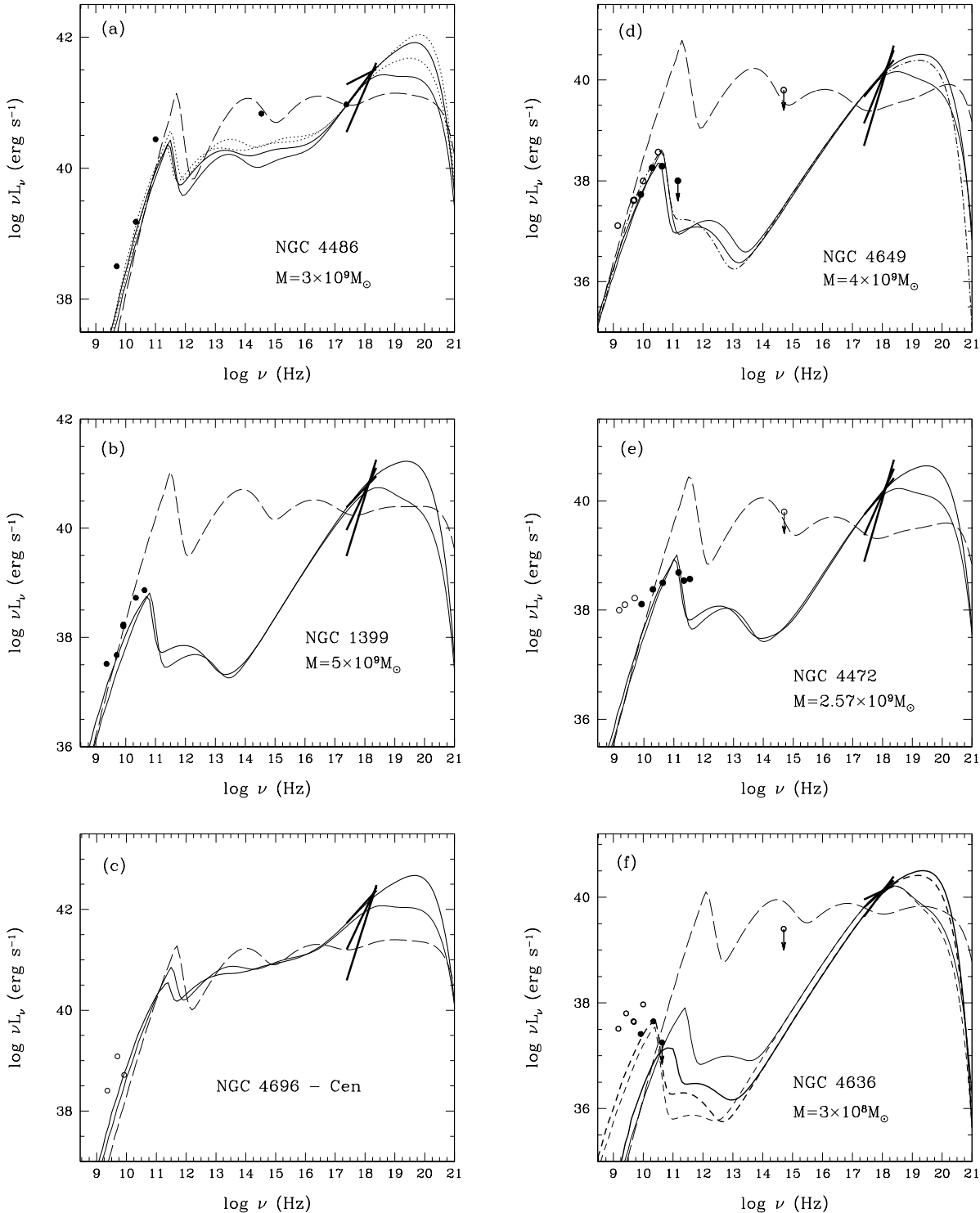


Figure 2. Spectral models calculated for ADAF models with and without winds. The central cluster galaxies are on the left-hand side and the Virgo elliptical galaxies are on the right-hand side. The model parameters, corresponding to the fits, are tabulated in Table 4. The long dashed line represents no-wind ADAFs; $p = 0$. The thicker solid line, models for $r_{\text{out}} \sim 300$. The thinner solid line, models for $r_{\text{out}} \sim 10^4$. The dotted lines in panel above and below the solid line (a) are for $r_{\text{out}} \sim 100$ and $r_{\text{out}} \sim 800$ respectively. The short dashed lines in panel (f) assume $m \sim 10^9$. The dash-dotted line in (d) is for a model with $\delta = 0.1$. Such models show better agreement with the characteristics radio spectrum. The solid dots represent the best constraint on the core emission. The thick solid lines the slopes and fluxes measured from the ASCA analysis (paper I). For the Virgo Cluster galaxies we assume a fixed luminosity distance of 18 Mpc. For NGC 1399 and 4696 the luminosity distances are calculated using the redshifts and an assumed cosmology of $H_0 = 50 \text{ km s}^{-1} \text{ Mpc}^{-1}$, $\Omega = 1$ and $\Lambda = 0$ (29 and 63 Mpc respectively).

7.2 Photon Starved Comptonization and Non-thermal Emission

In the above analysis we have assumed that the accreting plasma is thermal and that there is no contribution to the observed emission from non-thermal electrons. We have also assumed that any strong winds/outflows are non-radiative (this can be shown to be a plausible assumption within the context of a particular hydro-magnetic wind; Blandford & Payne 1982). Nevertheless, dissipation (in a flow/outflow with a shearing, near-equipartition, magnetic field) is likely to occur and, at least in part, it will do so in transient localized regions (behind shocks in the outflow or in sites of reconnection both in the flow and outflow) where a small number of electrons achieve ultra-relativistic energies. These electrons would cool much more rapidly and their synchrotron emission would extend to much higher energies (particularly if Comptonization is important) than for thermal electrons. The efficiency of these processes would be much higher, implying (in order to reproduce the observed low-luminosities) that either the accretion rates (i.e., the densities) are much lower than expected from the estimates given in Section 1, or that such processes accelerate only small number of particles in localized regions.

The observed radio spectrum and, in particular, its extension to the infrared (and possible higher frequencies), depends on how efficiently non-thermal particles can be accelerated. The fairly sharp cut-offs implied by the VLA and SCUBA observations (of the Virgo ellipticals and NGC 1399 - but not M87) imply that any synchrotron emission from a non-thermal distribution is unlikely to contribute significantly beyond ~ 10 GHz and therefore will not extend to X-ray energies.

One possible non-thermal model for the observed emission is that the same population of electrons produces both the radio/sub-mm emission by synchrotron radiation and the X-ray emission by the inverse Compton process. In this case, we can describe the relativistic electrons by a broken power-law distribution function, with spectral indices smaller and larger than 3, below and above a break energy γ_b (in units of $m_e c^2$), respectively (e.g. $N(\gamma) \propto \gamma^{-n_1,2}$ with $n_1 \sim 1 - 1.5$ for $\gamma < \gamma_b$ and $n_2 \sim 3 - 4$ for $\gamma > \gamma_b$). The peak of the synchrotron emission occurs at $\nu_S \approx (4/3)\nu_B\gamma_b^2$, where $\nu_B = 2.8 \times 10^6 B$ Hz is the Larmor frequency.

The observed spectral energy distributions for our sources indicate that the luminosity of the soft/synchrotron emission is typically a few orders of magnitude less than the X-ray luminosity, implying that the Compton spectra would arise from a photon starved plasma. The situation envisaged here resembles the synchrotron-self Compton model developed for BL Lac sources (e.g., Ghisellini 1989; Ghisellini, Maraschi & Dondi 1996; Ghisellini et al. 1998; in BL Lacs, Compton scattering of other soft photons, such as those arising from a standard accretion disk or the broad line region, can also be important; neither of these are, however, thought to be present in the elliptical galaxies of interest). ¶

¶ One crucial difference, however, is the absence of a radio cutoff in the spectrum of BL Lacs. This has important implications for the inferred parameters of nonthermal models, as is discussed below.

In those models (and others developed within the context of non-thermal photon starved - electron or pair - plasmas; Zdziarski & Lamb 1986; Zdziarski, Coppi & Lamb 1990) the sources are very compact (where the compactness parameter is defined by $\ell = L/R(\sigma_T/mc^3)$) which implies that all of the particles cool before escaping the source ($t_{\text{cool}} \sim \pi t_{\text{cross}}[\ell(\gamma - 1)]^{-1}$ and $t_{\text{cross}} \sim R/c$). A steady state can therefore be achieved.

A steep particle distribution is continuously injected; due to self-absorption, synchrotron cannot emit the bulk of this luminosity; in this case, it is primarily produced by multiple Compton scatterings (and flat X-ray energy indices $\ll 1$ can be obtained). For the sources in ellipticals, however, $\ell < 1$ even when $r = 1$. It is therefore difficult to have an optical depth close to unity and for multiple Compton scatterings to be important.

The injected power in non-thermal electrons can nonetheless still be greater than the synchrotron luminosity and would emerge as first order Compton scattering peaking at X-ray wavelengths. The maximum power in Inverse Compton emission will occur at a frequency $\nu_C \approx (4/3)\gamma_b^2\nu_S$ where, from observations, $\nu_C \gtrsim 10$ keV. Given the frequency of the radio peak and a lower limit for ν_C we can derive the energy of the electrons contributing most of the power and the required magnetic field strength: $\gamma_b \approx (3\nu_C/[4\nu_S])^{1/2} \sim 10^4$ and $B \sim 10^{-5}$ Gauss.

The required magnetic field strength $\sim 10^{-5}$ Gauss is an implausibly small fraction of the equipartition value for the accretion flow (even in the presence of a strong wind, $B_{\text{equi}} \sim 1$ Gauss near $r \sim 1$). Thus, it is unlikely that non-thermal synchrotron self-Compton processes in the accretion flow are important contributors to the observed emission. It is also not likely that field strengths as low as $\sim 10^{-5}$ Gauss could be achieved in an outflow/wind or jet. Equipartition with the radiation energy density (in particular for localized regions) would still predict much higher field strengths. In any case, for such photon starved cases bremsstrahlung emission from both a thermal or non-thermal population is likely to be important. If the X-ray emission were due to e.g. second (or third) order Compton scattering (for a similarly peaked electron distribution but with $\gamma_b \sim$ a few 100), the limits on B would be relaxed. In order for the second order Compton scattering to contain the required X-ray luminosity, τ would need to be high (e.g. ~ 1 , since the probability for a second order Compton scattering scales as τ^2). Given the observational constraint that $\ell \ll 1$, large enough optical depths would seem difficult to achieve (given the highly sub-Eddington nature of the sources the 'jet' emitting region needs to be localized and have low density).

We note that the case is different for M87. For this object a sharp spectral turnover in the radio band is not required by the data (see Fig. 2a). The spectral energy distribution (radio, optical data and the hard X-ray spectra) is still somewhat double peaked but with similar luminosities in both the radio-optical and X-ray peaks. From above, for $\gamma_b \sim 100$ (and assuming a lower limit for the high energy peak to be around 10 keV, although contributions up to gamma-ray frequencies are likely to occur), the magnetic field can be much larger than in the previous cases, comparable to the equipartition value. We cannot, therefore, exclude some relevant contribution to the spectral energy distribution from non-thermal particles in M87. Note, although, that

the highly sub-Eddington luminosity of this source still puts very strong constraints on the density and emitting region size.

In conclusion, simple estimates of non-thermal synchrotron self-Compton models for the observed radio and X-ray emission in nearby ellipticals suggest that highly sub-equipartition magnetic fields are required ($B \sim 10^{-5}$ Gauss). This is contrary to expectations, both for the accretion flow and for a magnetically driven wind or a collimated outflow. We cannot, however, rule out other non-thermal models for the observed emission such as a jet seen off-axis with separate populations of nonthermal electrons producing the observed radio and X-ray emission by synchrotron radiation, or an unobserved source of soft photons in the optical/IR available for Compton scattering, etc. Although these might quickly become rather contrived.

The most promising means of distinguishing bremsstrahlung and non-thermal models is likely to be variability, which is discussed in the next section.

8 VARIABILITY

Here we give a brief discussion of the variability properties of the bremsstrahlung model, the salient feature of which is that *there should be little to no short timescale (\sim day to month) X-ray variability because the bremsstrahlung emission arises from relatively large radii in the accretion flow.*

The bremsstrahlung emission from a radius r in the accretion flow can be expected to vary by (at most) order unity on a timescale comparable to the local dynamical time, given by $t_d \approx (R^3/GM)^{1/2} \approx 4m_9 r^{3/2}$ hours.^{||} For timescales less than $t_d(r)$ the variability from emission at radius r is suppressed. An upper limit to the suppression can be made by noting that for $t' < t_d(r)$, there can still be (at most) order unity variability from fluctuations on length scales $r' \approx v_K(r)t'$. There are $\sim (r/r')^3$ such blobs varying incoherently in a shell of radius r and thickness $dr \sim r$. Consequently, for $t' < t_d(r)$, the variability amplitude should be $< [t'/t_d(r)]^{3/2}$. This is a strict upper limit because in reality there will be a power spectrum of fluctuations with small scale fluctuations having less power than large scale fluctuations.

The above analysis implies that the fractional luminosity fluctuation at frequency ν on a timescale δt is given by

$$\frac{\delta L_\nu(\delta t)}{L_\nu} = \frac{\int d\log r \epsilon_\nu(r) W(r, \delta t)}{\int d\log r \epsilon_\nu(r)}, \quad (6)$$

where ϵ_ν is the bremsstrahlung emissivity (examples of which are in Figure 1) and

$$W(r, \delta t) = A \text{ Min} \left(1, \left[\frac{\delta t}{t_d(r)} \right]^{3/2} \right) \quad (7)$$

is the power spectrum for the particular model given above ($A \sim 1$ is the amplitude of the fluctuation on the dynamical time).^{**}

^{||} For bremsstrahlung, it is the dynamical time, not the light crossing time, which is relevant.

^{**} If, as they should be, the bremsstrahlung emissivity fluctua-

A crude approximation to the above integral can be obtained by setting $\epsilon_\nu(r) \propto \delta(r - r_\nu)$, where r_ν is the radius near which most of the emission at frequency ν originates. In this case,

$$\frac{\delta L_\nu(\delta t)}{L_\nu} \sim A \text{ Min} \left(1, \left[\frac{\delta t}{t_d(r_\nu)} \right]^{3/2} \right). \quad (8)$$

Even in the absence of a wind, $r_\nu \gtrsim 100$ for all X-ray energies of interest (see Fig. 1). In fact, in the soft X-rays (~ 1 keV), $r_\nu \approx 10^3 - 10^4$. For wind models, the value of r_ν in the soft X-rays is unchanged while in the hard X-rays ($\gtrsim 10$ keV) it becomes $r_\nu \approx r_{\text{out}}$. That is, the bremsstrahlung emission in the hard X-rays is dominated by the radius at which the wind becomes important (see Fig. 1b). Consequently, variability studies at $\gtrsim 10$ keV can explicitly determine the value of r_{out} .

For $r_\nu \sim 100$, the dynamical time is ≈ 1 year. It is clear, then, that within the bremsstrahlung interpretation there should be no variability in the observed X-rays over a single observing run. Furthermore, multiple observing runs should detect significant variability only if separated by months or even years.

To be slightly more explicit, Figure 3 shows the expected variability (calculated from eq. [6]) for five X-ray energies for the model whose emissivity curves are shown by dotted lines in Figure 1, namely a model with a wind with $r_{\text{out}} = 10^3$ and $p = 0.5$ (recall that these are observationally favored parameters). This model assumes that only bremsstrahlung contributes to the X-ray emission (no Comptonization or nonthermal particle emission). Note that the relevant dimensionless variability timescale is $\delta t/t_d(r) \propto \delta t/m_9$ (hence the abscissa in Fig. 3).

For $\delta t \sim$ a day, the luminosity fluctuation expected is $\lesssim 0.1\%$. Even for $\delta t \sim$ a month, $\delta L_\nu/L_\nu \lesssim 10\%$ around 100 keV and $\delta L_\nu/L_\nu \lesssim 0.3\%$ around 1 keV. Only on a timescale of \sim a year do we expect significant X-ray variability. Note also the clear trend with X-ray energy: the variability is greater at higher X-ray energies since this emission arises from closer to the black hole.

Observations of short timescale variability would imply that either the flow is highly inhomogeneous and bremsstrahlung emission is produced in localized, higher density regions or that non-thermal SSC of thermal Comptonization in the central region is producing the observed flux.

One further diagnostic for testing the bremsstrahlung hypothesis is the observations of thermal X-ray lines, a test that should be plausibly carried out with the Chandra Observatory (Narayan & Raymond 1999). If the X-ray emission is dominated by the bremsstrahlung emission the X-ray spectrum of the accretion flow should exhibit thermal X-ray lines (Narayan & Raymond 1999). Their presence would also be an important discriminant for assessing the outer radius of the flow (because of the strong temperature dependence and the one-to-one mapping between temperature and radius the bulk of the line emission is expected to originate from radii outside 10^4 ; Narayan & Raymond 1999).

tions are due to density fluctuations, the 3/2 power law in equation (7) becomes 3/2 + 2/3 (for Kolmogorov turbulence, either hydrodynamic or magneto-hydrodynamic).

8.1 M87

ROSAT HRI observations (~ 1 keV) of the “core” of M87 show $\approx 20\%$ variability on timescales of ≈ 6 months to a year (Harris, Biretta, & Junor 1997). This is not easy to reconcile with a wind-dominated bremsstrahlung model for the X-ray emission. For M87, $m_9 \approx 3$. Thus, if a model with $p \approx 0.5$ and $r_{\text{out}} \approx 10^3$ is appropriate for M87, bremsstrahlung alone would lead to $\lesssim 1\%$ variability at ≈ 1 keV on timescales of \approx a year (cf Fig. 3), inconsistent with the observations.

One possible resolution of this discrepancy is that r_{out} is $\ll 10^3$ so that there is significant X-ray emission from closer to the black hole. We find that if $r_{\text{out}} \lesssim 30$, $\sim 10\%$ soft X-ray variability can be produced (note from Fig. 1a that there is a $\sim 10\%$ contribution to the soft X-ray bremsstrahlung luminosity from $r \sim 10$ in the absence of a wind). If such a small value of r_{out} is applicable to all of the members of our sample, however, very large values of $p \gtrsim 1$ are required to reproduce the observed X-ray to radio luminosity ratios (note that this is *not* required for M87).

As emphasized in previous sections, however, M87 is a peculiar member of our sample. It is the only system for which high frequency radio observations do not show a strong suppression (and therefore there are no strong arguments against significant emission from nonthermal particles; see the previous section). Its one sided jet, likely to be pointing towards us, is known to contribute to the emission in the very core region (Baath et al. 1992) and to produce X-rays (knot A has a slightly smaller X-ray luminosity than the core; Harris et al. 1997)

The “core emission” in this case is likely to contain significant contamination from unresolved jet emission, in addition to accretion flow emission. This is likely the origin of the variable soft X-ray emission. Two reasons argue against thinking that all of the X-ray emission is due to unresolved jet emission with a negligible accretion flow contribution. (1) Accretion at the Bondi rate in M87 should produce an X-ray luminosity comparable to that observed and (2) there is a clear correlation between the hard power law X-ray emission and the host galaxy X-ray emission in the six ellipticals we are studying (cf Fig. 3 of Paper 1 and discussion therein). Excluding M87, these systems are not believed to have jets which can produce hard X-rays at the level observed. Since M87 nicely satisfies the observed correlation, the non-jet emission should therefore be comparable to the total emission.

For a number of reasons, M87 is therefore a poor system in which to probe the (lack of) variability expected from bremsstrahlung emission in our models. More promising candidates are the Virgo ellipticals (NGC 4472, 4636, and 4649). The large X-ray/radio luminosity ratios in these systems (in contrast to M87) imply negligible contributions from Comptonized synchrotron photons in the X-ray band. Jet emission in X-rays is also expected to be small in these systems. Barring nonthermal particle emission from the accretion flow/wind (see §7), the X-ray emission should therefore be dominated by bremsstrahlung processes, providing an excellent test of our variability predictions.

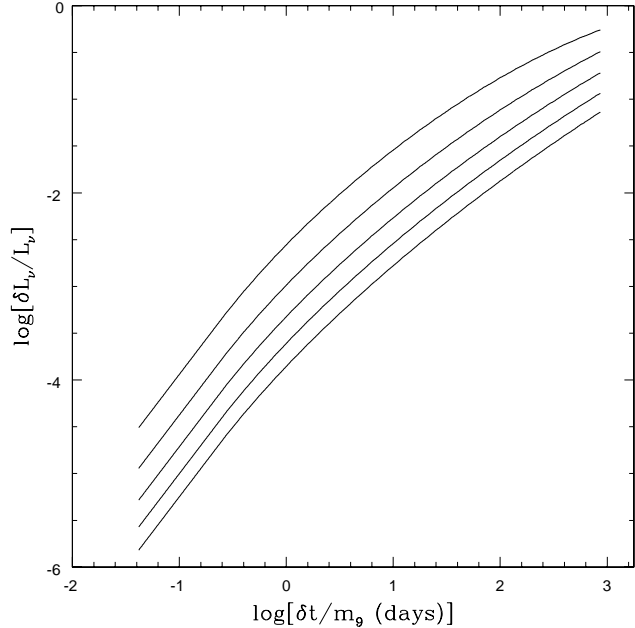


Figure 3. The fractional variability expected at five X-ray energies (100, 30, 10, 3 & 1 keV, from top to bottom) as a function of the timescale of observation in days. The figure assumes pure bremsstrahlung emission in the X-ray band and a spectral model with $p = 0.5$ and $r_{\text{out}} = 10^3$.

9 SUMMARY AND DISCUSSION

The discovery of hard power-law emission (Paper I) from a sample of elliptical galaxies has brought to a sharper focus the study of nearby supermassive quiescent black holes. We have discussed how the broad band spectral energy distributions of this sample of elliptical galaxies, accreting from their hot gaseous halos at rates comparable to their Bondi rates, can be explained by low-radiative efficiency accretion flows in which a significant fraction of the mass, angular momentum and energy is removed from the flows by winds. Such outflows are not simply an added parameter in the model but a dynamically important component of accretion at low radiative efficiency (Blandford & Begelman 1999). The characteristically suppressed synchrotron emission in the radio band (excluding M87) and the systematically hard X-ray spectra, as expected from thermal bremsstrahlung processes, strongly supports the conjecture that significant mass outflow is a natural consequence of systems accreting at low-radiative efficiencies.

Bremsstrahlung emission in the 2–10 keV band is produced primarily at large radii in the accretion flow and is sensitive to the rate at which matter is fed to the flow (\dot{m}_{out}). By contrast, synchrotron emission originates from the interior regions and, for a given value of \dot{m}_{out} , decreases significantly with increasing p (where p is the power-law index of the accretion rate in the flow, i.e., $\dot{m} \propto \dot{m}_{\text{out}}(r/r_{\text{out}}^p)$ for $r < r_{\text{out}}$). We have shown that radio observations (DM99) and ASCA X-ray fluxes can be explained by ADAF models only if \dot{m}_{out} is of order the Bondi value $\sim 0.001 - 0.02$, $p \sim 0.5 - 1$ and $r_{\text{out}} \sim 100 - 1000$. Significant electron heating (e.g. $\delta \gtrsim 0.1$) is also fully consistent with the outflow

models for ellipticals. In view of this, Sgr* A might not be very different from the elliptical nuclei we have studied here and can also be explained within the context of strong mass loss models (with the strict requirement, in order to satisfy the firm VLBI constraints, that $\delta \gtrsim 0.1$ in the Galactic centre; see QN99).

The small values of r_{out} relative to the accretion radius ($r_A \sim 10^6$) may suggest that angular momentum only becomes important well inside the accretion radius.

We have examined possible contributions from non-thermal particle distributions (which are likely to originate in shock regions and reconnection sites in the flow/outflows, or in the observed jets). The observed lack of any extension of the synchrotron component towards IR and optical wavelengths, and the typically high ratio of X-ray to radio luminosity (in the Virgo ellipticals and NGC1399), places strong limits on the magnetic fields strengths, implying that any non-thermal components are unlikely to contribute significantly to the observed emission. A bremsstrahlung component is more likely to dominate the X-ray emission than SSC. The case of M87 is less clear and non-thermal contributions, both at low and high energies, may occur. However, the highly sub-Eddington luminosity of M87 (and the other galaxies in our sample) does not allow a simple connection with jet dominated, Blazar-like sources to be made. Theoretical models and observations at higher energies (e.g. gamma rays) are required to better assess the importance of non-thermal models. Outflows, if present, should contain most of the energy and mass but need to be very radiatively inefficient.

The predicted absence of short timescale variability in the X-ray band, which is expected if the X-ray emission is primarily bremsstrahlung emission (which in wind models originate from $r_{\text{out}} \sim 100 - 1000$, where the dynamical timescale is months to years) will be readily assessed with observations made with the Chandra observatory. If the X-ray emission is dominated by bremsstrahlung processes, the X-ray spectrum may also exhibit thermal line emission (Narayan & Raymond 1999). Their presence would also be an important discriminant for assessing the outer radius of the flow (because of the strong temperature dependence and the one-to-one mapping between temperature and radius, the bulk of the line emission is expected to originate from radii outside 10^4 ; Narayan & Raymond 1999).

As discussed in Paper I, even from a purely observational point of view, the low luminosities of the sources we are considering and their characteristically hard and energetically dominant X-ray spectra, identify the elliptical galaxy nuclei as a new class of accreting black holes, which can be clearly distinguished from Seyfert nuclei (which are most often hosted in spiral galaxies). We suggest that the difference in radiative efficiency (readily assessed in ellipticals given the black hole mass and estimates of accretion rates), manifested by the accretion flows close to the black holes, in these different classes of objects, does not solely arise from a difference in \dot{m} (the Bondi rates are adequate to fuel an active nucleus in the elliptical galaxies and a thin disk solution would be viable).

The accretion solution adopted is likely to depend on the manner in which material is fed into the nucleus (e.g. Rees et al. 1982; Begelman 1986). In spiral galaxies, the bulk of the interstellar medium resides in a disk and it is plausi-

ble that a radiatively efficient flow persists all the way into the black hole. In elliptical galaxies, most of the gas participating in the angular momentum-dominated accretion flow originates from the hot interstellar medium that pervades the galaxies (often forming a cooling flow). We have speculated that the increase in magnetic field strength due to the radial inflow and shear in a cooling flow (with the magnetic field pressure in equipartition with thermal pressure within radii ~ 10 kpc) might be the primary cause for the ensuing high α accretion flow. (Material fed into the accretion flow would be highly magnetized and α should scale \propto to magnetic field strength; e.g. Hawley et al. 1996). High viscosity parameters (if $\alpha \sim 0.1$ can be achieved) would in turn give rise to low-radiative efficiencies. The presence of relatively strong magnetic fields in these environments can also play an important role for driving and possibly collimating the outflows. We suggest that the outflows could be energized by loops of field anchored to the flow itself (and responsible for driving the wind). At large distances from the disk, the inertia of the gas can cause the magnetic field to become increasingly toroidal. Magnetic stresses could be responsible for converting the centrifugal outflow into a more collimated jet structure. The development of radio structures in ellipticals may also be fostered by the presence of a hot interstellar medium (and the more prominent radio structures in central cluster galaxies - the FRI type sources in the sample - are the ones to be found in the gas richer, higher pressure environments; see also Fig. 3 in Paper I) and partially suppressed by its absence in spirals. We note that, if not partially collimated, an outflow (which would contain most of the accreted mass, $\sim 90 - 97$ per cent) could stifle the accretion flow. If accretion is stifled the radio and X-ray emission are likely to be produced by small numbers of non-thermal particles in shock sites in the jets/outflows.

We further argue that low-radiative efficiency accretion and its associated outflows maybe relevant for understanding radio-loud AGN. We are suggesting that the more active M87, a classical FRI source (see also Reynolds et al. 1996) together with NGC 1399 and NGC 4696 (also weak FRI sources) provide us with some of the strongest evidence for low-efficiency accretion. X-ray emission from FR-II sources is often associated with the presence of broad iron $K\alpha$ fluorescence lines and therefore thin accretion disks (e.g. 3C 109, Allen et al. 1996; 3C390.3 Eracleous, Halpern & Livio 1996). The difference in accretion mode (e.g. see also Begelman 1985) may also be manifested in the different properties of FRI and FR-II sources.

The differences between elliptical and spiral nuclei does not only arise from their different environments but also from their respective histories: elliptical galaxies have black hole masses of $10^9 - 10^{10} M_{\odot}$, consistent with those expected if these galaxies have undergone a quasar phase in the past (e.g. Salucci et al. 1998). Black holes in spiral galaxies do not exceed $10^8 M_{\odot}$, supporting the suggestion that accretion at low-radiative efficiencies might be relevant in the final stages of accretion in early type galaxies.

ACKNOWLEDGMENTS

We thank Chris Carilli for the high frequency VLA data of NGC 1399 and Dimitrios Psaltis for very useful conver-

sations. TDM acknowledges support for this work provided by NASA through Chandra Postdoctoral Fellowship grant number PF8-10005 awarded by the Chandra Science Center, which is operated by the Smithsonian Astrophysical Observatory for NASA under contract NAS8-39073. E.Q. is supported by NSF Graduate Research Fellowship.

REFERENCES

Allen S.W., Di Matteo T., Fabian A.C., 1999, MNRAS, submitted (Paper 1)

Allen S.W., Fabian A.C., Idesawa E., Inoue H., Kii T., Otani C., 1997, MNRAS, 286, 765

Abramowicz M., Chen X., Kato S., Lasota J. P., Regev O., 1995, ApJ, 438, L37

Balbus, S. A., Hawley, J. F., in *Accretion Processes in Astrophysical Systems: Some Like it Hot!* Eighth Astrophysics Conference, College Park, MD, October 1997. Edited by Stephen S. Holt and Timothy R. Kallman, AIP Conference Proceedings 431., p.79

Begelman M. C., 1985, in *Astrophysics of active galaxies and quasi-stellar objects*, eds Miller J. S., University Science Books, Mill Valley, P411

Begelman M. C., 1986, Nat, 322, 614

Bisnovatyi-Kogan, G.S., Lovelace, R.V.E., 1997, ApJ, 486, L43

Blackman E.G., 1999, MNRAS, 302, 723

Blandford R.D., Begelman M.C., 1999, MNRAS, 303, L1

Blandford R.D., Payne D.G., 1982, MNRAS, 199, 883

Bondi H., 1952, MNRAS, 112, 195

Byun Y., et al. 1996, AJ, 111, 1889

Chandran B., Cowley S., Sydora R., 1997, AAS, 191, 5307

Di Matteo T., Fabian A.C., 1997, MNRAS, 286, L50

Di Matteo T., Fabian A.C., 1997a, MNRAS, 286, 393

Di Matteo T., Fabian A.C., Rees M.J., Carilli C.L., Ivison R.J., 1999, MNRAS, in press

Eracleous M., Halpern J.P., Livio M., 1996, ApJ, 459, 89

Esin A.A., McClintock J.E., Narayan R., 1997, ApJ, 489, 865

Fabian A. C., Canizares C. R., 1988, Nat, 333, 829

Fabian A. C., Rees M. J., 1995, MNRAS, 277, L55

Fabbiano G., Kim D.W., Trinchieri G., ApJS, 1992, 80, 531

Ford H. C. et al. 1995, ApJ, 1994, 435, L27

Ghisellini G., 1989, MNRAS, 236, 341

Ghisellini G., Maraschi L., Dondi L., 1996, A&A Suppl. S., 120, 503

Ghisellini G., Celotti A., Fossati G., Maraschi L., Comastri A., 1998, MNRAS, 301, 451

Gruzinov A. V., 1999, ApJ, submitted

Gruzinov A. V., 1998, ApJ, 1998, ApJ, 501, 787

Harms R. J. et al., 1994, ApJ, 435, L35

Hawley J. F., Gammie C. F., Balbus, S. A., 1996, 464, 690

Ho, L. C. 1998, in *Observational Evidence for Black Holes in the Universe*, ed. S. K. Chakrabarti (Dordrecht: Kluwer), 157

Hummel E., Kotani C. G., Ekers R. D., 1983, A&A, 127, 205

Kormendy J., Richstone D. 1995, ARA&A, 33, 581

Macchetto, F., Marconi A., Axon D.J., Capetti A., Sparks W., Crane P., 1997, ApJ, 489, 579

Magorrian J. et al., 1998, AJ, 115, 2285

Mahadevan R., 1997, ApJ, 477, 585

McKee, C.F., Cowie L.L., 1977, ApJ, 215, 213

Meszaros P., A&A, 44, 59

Nakamura K.E., Kusunose M., Matsumoto R., Kato S., 1997, PASJ, 49, 503

Narayan R., Yi I., 1994, ApJ, 428, L13

Narayan R., Yi I., 1995a, ApJ, 444, 231 bibitem Narayan R., Yi I., 1995b, ApJ, 452, 710

Narayan R., Raymond J., 1999, ApJ, 515, L69

Narayan R., Barret D., McClintock J., 1997, ApJ, 482, 448

Narayan R., Mahadevan R., Quataert E., 1998, to appear in "The Theory of Black Hole Accretion Discs", eds. M. A. Abramowicz, G. Bjornsson, and J. E. Pringle, (Cambridge University Press)

Nulsen P.E.J., Stewart G.C., Fabian A.C., 1984, 208, 185

Quataert E., 1998, ApJ, 500, 978

Quataert E., Gruzinov A.V., 1999, ApJ, in press

Quataert E., Narayan R., 1999, ApJ, in press

Rees M. J., 1982, in Riegler G., Blandford R., eds, *The Galactic Center*. Am. Inst. Phys., New York, 166

Rees M.J., 1987, MNRAS, 228, 47p

Rees M. J., Begelman M. C., Blandford R. D., Phinney E. S., 1982, NAT., 295, 17

Reynolds C. S., Di Matteo T., Fabian A. C., Hwang U., Canizares C. R., 1997, MNRAS, 283, L111

Sadler E. M., Jenkins C. R., Kotanji C. G., 1989, MNRAS, 240, 591

Salucci P., Szuszkiewicz E., Monaco P., Danese L., 1998, MNRAS submitted

Shapiro S.L., 1973, ApJ, 185, 69

Slee O. B., Sadler E. M., Reynolds J. E., Ekers R. D., 1994, MNRAS, 269, 928

Soker N., Sarazin C., 1990, ApJ, 348, 73

Stewart G.C., Canizares C.R., Fabian A.C., Nulsen P.E.J., ApJ, 278, 536

Wrobel J. M., 1991, AJ, 101, 127

Wrobel J.M., Heeschen D.S., 1991, AJ, 101, 148

Van der Marel R.P., 1991, MNRAS, 253, 710

van der Marel R.P., 1998, ApJ, submitted, (astro-ph/9806365)

Zdziarski A., Lamb D.Q., 1986, 309, L79

Zdziarski A., Coppi P.S., Lamb D.Q., 1990, ApJ, 357, 149